

# Structural and Magnetic Study of Active Screen Plasma Nitrided $Fe_{73.5}Si_{13.5}B_9Nb_3Cu_1$ and $Fe_{77}Si_{11}B_9Nb_{2.4}Cu_{0.6}$ Ribbons

E. Memarzadeh Lotfabad<sup>1</sup>, H.R. Madaah Hosseini<sup>1,\*</sup>,  
H. Asghari Shivaee<sup>2</sup> and S. Roostaie<sup>3</sup>

**Abstract.** The comparative study of Active Screen Plasma Nitriding (ASP) treatment of two Finemet-type alloys with the compositions of  $Fe_{73.5}Si_{13.5}B_9Nb_3Cu_1$  and  $Fe_{77}Si_{11}B_9Nb_{2.4}Cu_{0.6}$  was investigated in different temperatures ranging from  $410^\circ C$  to  $560^\circ C$ . Differential Scanning Calorimetry (DSC), X-Ray Diffractometry (XRD), Atomic Force Microscopy (AFM), Scanning Electron Microscopy (SEM), electrical resistivity, microhardness measurements and magnetic characterization by a Vibrating Sample Magnetometer (VSM) were utilized to characterize the treated samples. The comparison of the DSC data for the alloys suggested that the smaller amount of Nb as a growth inhibitor shifted the crystallization temperatures towards lower temperatures. Thus, the crystalline volume fraction and grain size in each temperature for  $Fe_{77}Si_{11}B_9Nb_{2.4}Cu_{0.6}$  alloy increased compared to  $Fe_{73.5}Si_{13.5}B_9Nb_3Cu_1$  alloy. The size of iron nitrides on the surface of the ribbons with the lower Si content was larger. The electrical resistivity for the annealed and nitrided  $Fe_{77}Si_{11}B_9Nb_{2.4}Cu_{0.6}$  alloy was lower compared to the annealed and nitrided  $Fe_{73.5}Si_{13.5}B_9Nb_3Cu_1$  alloy, due to the larger grain size and lower Si content of Fe(Si) phase in  $Fe_{77}Si_{11}B_9Nb_{2.4}Cu_{0.6}$  alloy. The VSM results showed that the maximum saturation magnetization and coercivity at  $440^\circ C$  were obtained in  $Fe_{77}Si_{11}B_9Nb_{2.4}Cu_{0.6}$  alloy after nitriding under 75%  $H_2$  and 75%  $N_2$  gas mixture, respectively.

**Keywords:** Fe-Si-Nb-B-Cu alloys; Comparative study; Crystallization; Active screen plasma nitriding.

## INTRODUCTION

The Fe-Cu-Nb-Si-B finemet alloys exhibit excellent soft magnetic properties due to nanocrystalline  $\alpha$ -Fe(Si) grains dispersed in a residual amorphous matrix [1,2]. These alloys are derived from the conventional Fe-Si-B system with minor additions of copper (Cu) and niobium (Nb). In this case, Cu acts as nucleating agent, whereas Nb inhibits the grain growth of the FeSi phase that crystallizes from the amorphous matrix during annealing. The Finemet alloys

are prepared by the melt-spinning technique followed by annealing at elevated temperatures to achieve a nanocrystalline structure [2,3]. Their magnetic properties depend on chemical compositions and also are able to be optimized by applying a heat treatment in temperature ranges close to the crystallization temperature [4]. Koster and Meinhardt [5] studied primary crystallization of Finemet alloys and found that the growth of nanocrystals can be controlled by selecting proper composition. Changes in the type or content of elements in Finemet alloys are known to be one way to improve magnetic, corrosion and mechanical properties [6,7]. The method and condition of nanocrystallization treatment have also important role in the formation of the nanocrystalline state [8]. Although classical thermal treatments under vacuum are used commonly, thermo-chemical treatments which are used in the steel industry also can be applied. These treatments act by thermal diffusion of one or more external elements. In nitriding thermo-chemical treatment, the element used is nitrogen which results

1. Department of Materials Science and Engineering, Sharif University of Technology, Tehran, P.O. Box 11155-9466, Iran.

2. Institute for Nanoscience and Nanotechnology, Sharif University of Technology, Tehran, P.O. Box 14588-89694, Iran.

3. Department of Mining and Metallurgical Engineering, Amir Kabir University of Technology, P.O. Box 15875-4413, Tehran, Iran.

\*. Corresponding author. Email: madaah@sharif.edu

Received 16 February 2010; received in revised form 13 April 2010; accepted 21 August 2010

in the improvement of some mechanical properties. The diffusion of nitrogen atoms and chemical surface modifications produce structural modifications leading to substantial improvements in the properties of the material [8,9]. Gas Nitriding (GN) treatment gives a slightly improved nanocrystalline state by decreasing the  $\alpha$ -Fe(Si) grain size and increasing the crystalline volume fraction in Finemet ribbons which results in decreasing the magnetostriction. However, using the higher parameters of crystallization (520°C and 6 h) than those commonly used in the conventional treatment (500°C and 1 h) results in significantly higher coercivity for the gas nitrided samples [8].

Plasma nitriding process is widely used and has a number of distinct advantages over the gas nitriding treatment, for example the non-emission of pollutants, energy economy and lesser treatment time [10]. Furthermore, it can be applied in lower temperatures due to plasma activation. After nitriding, a thin compound layer is produced on the component surface and a nitrogen diffusion layer is formed beneath it. The extent of surface hardness increasing depends on the process parameters, such as temperature, atmosphere and the alloying elements in substrate. In common plasma nitriding, the components are heated as a result of ion bombardment on the surface. The components with different shape or different ratio of surface to mass may undergo different ion bombardment intensity. As a result, the inhomogeneous temperature distribution occurs on different components or different parts and hardness and depth of nitrogen diffusion after plasma nitriding are inhomogeneous [11]. In order to reduce the effect of the above-mentioned disadvantages, some new processes were developed. Recently, a method named "Active Screen Plasma Nitriding" (ASPN) is introduced in which the specimens are placed inside a cylindrical steel screen on which cathodic potential is applied, leading to formation of plasma on the screen not on the specimens, and the required heat for the process is supplied from the screen radiation [11-13].

The aim of this study is to compare the structural, mechanical, electrical and magnetic properties of two types of crystallized Finemet amorphous ribbons with the compositions of  $\text{Fe}_{73.5}\text{Si}_{13.5}\text{B}_9\text{Nb}_3\text{Cu}_1$  and  $\text{Fe}_{77}\text{Si}_{11}\text{B}_9\text{Nb}_{2.4}\text{Cu}_{0.6}$  submitted to ASPN and conventional annealing treatment.

## EXPERIMENTAL PROCEDURE

The amorphous ribbons with a cross-section of about 0.02 mm  $\times$  1 mm and the nominal compositions  $\text{Fe}_{73.5}\text{Si}_{13.5}\text{B}_9\text{Nb}_3\text{Cu}$  (hereafter denoted F1 sample) and  $\text{Fe}_{77}\text{Si}_{11}\text{B}_9\text{Nb}_{2.4}\text{Cu}_{0.6}$  (hereafter denoted F2 sample) have been prepared by rapid quenching of the melt. The primary alloys were prepared from high purity elements by arc melting under Argon (Ar)

atmosphere and then three times remelted. For melt spinning, the alloys were remelted in a quartz tube followed by ejecting through a nozzle onto a rotating Cu wheel. The composition of the initial amorphous precursor ribbons was determined using an Inductively Coupled Plasma (ICP) chemical analysis method. The crystallization processes have been monitored using the Differential Scanning Calorimetry (DSC). DSC thermo-analyses have been performed with a Mettler Toledo DSC-1 device with a heating rate of 5°C/min up to 700°C. The ASPN treatment was performed using a horizontal mounted cylindrical stainless steel vacuum chamber (diameter: 70 cm; length=80 cm) equipped with a plain carbon steel cylinder of active screen that worked as a cathode (diameter: 100 mm; height=50 mm) with 2 mm thickness and the holes diameter of 8-9 mm. The F1 and F2 amorphous ribbons were subjected to ASPN treatment at 410, 440, 480, 520 and 560°C in 75%  $\text{N}_2$ -25%  $\text{H}_2$  and 75%  $\text{H}_2$ -25%  $\text{N}_2$  gas mixtures for 3 h. Samples were mounted on the stainless steel fixture and placed on the worktable surrounded by active screen. The vacuum chamber was the anode in discharge system. The temperature of the specimen was measured with a thermocouple inserted in the fixture in a vertical position. The temperature was controlled by varying the power supplied to the active screen. The working pressure was  $5\pm 1$  mbar and the pulse DC voltage of 500-600 V was applied on the active screen. The amorphous ribbons were then annealed in vacuum sealed quartz ampoules and placed in a furnace with the same conditions of temperatures and time. This enables a comparative study between two alloys in both ASPN and conventional annealing treatment.

The samples states (amorphous and nanocrystalline) and structures were checked with X-Ray Diffractometry (XRD) using Philips PW 1800 ( $\lambda=1.54056 \text{ \AA}$ ). Tscan Vega2 Scanning Electron Microscopy (SEM) with an Energy Dispersive Spectroscopy (EDS) was used to analyze the composition and elements distribution from surface to the center of the ribbons. Atomic Force Microscopy (AFM) was employed to compare the crystallization process and formed nitrided phases on the surface of the ribbons. The electrical resistivity of the ribbons was measured using Multimeter HIOKI 3256 ohm-meter device. The Vickers microhardness test with a load of 50 g was carried out. The magnetization curves of nitrided and annealed ribbons at room temperature were measured in a PAR-4500 Vibrating Sample Magnetometer (VSM).

## RESULTS AND DISCUSSION

Figure 1 shows the DSC results for F2 amorphous ribbon. As shown, two sets of strong exothermic peaks

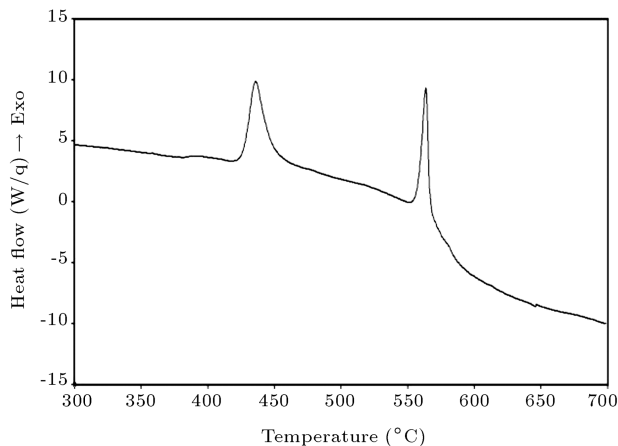


**Figure 1.** DSC curve of F2 amorphous ribbon measured at 5°C/min heating rate.

are detected. The values of the crystallization onset, end set and peak temperatures for both alloys are given in Table 1. For the F1 sample, the first peak appears at about 473°C which is attributed to the onset crystallization temperature of the nanocrystalline phase, i.e. Fe(Si) soft ferromagnetic phase, and the second one at 585°C related to the formation of iron boride phases, as already reported elsewhere [14]. The primary and the second crystallization peaks, for the F2 sample, however, appeared at two different temperatures, i.e. 426 and 557°C, respectively. As expected, the calorimetric behavior of the samples is quite different, depending upon composition of each sample. The comparison of the DSC data for two series of samples suggests that the smaller amount of Nb shifts the first and second crystallization peak towards lower temperatures. This is mainly due to the smaller amount of Nb that limits the growth of nanocrystals and acts as a stabilizer for the amorphous phase.

Figures 2 and 3 show XRD patterns of the as-spun, nitrided and annealed F1 and F2 samples. As can be realized from these patterns, for the as-spun samples only one broad peak around  $2\theta=45^\circ$  is noticeable, indicating that the sample is amorphous.

The XRD patterns of the F2 samples nitrided and annealed at 410°C (Figure 3a) exhibit three major diffraction lines corresponding to the (1,1,0), (2,0,0) and (2,1,1) reflections of the  $\alpha$ -Fe(Si) phase. It is expected to observe the diffusion of nitrogen from the surface to the interior depending on temperature, time and chemical composition of the alloy [15]. Diffusion

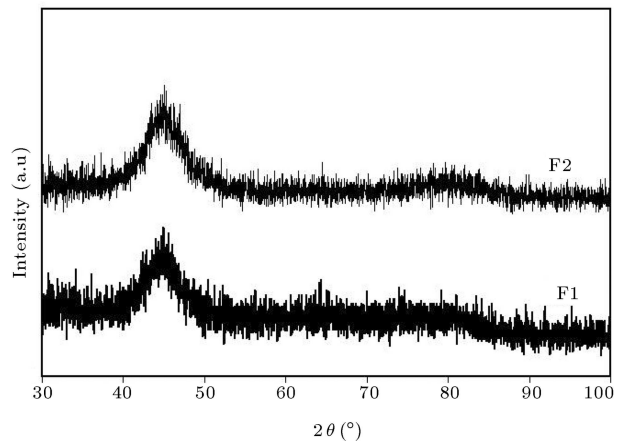


**Figure 2.** XRD patterns of the as-spun F1 and F2 samples.

of nitrogen was confirmed by XRD analysis. X-ray spectra showed the presence of nitrogen as  $\text{Fe}_4\text{N}$  and  $\text{Fe}_{2-3}\text{N}$ . But at this temperature, the nitrided and annealed F1 samples remained amorphous and only the  $\alpha$ -Fe(Si) nuclei were determined [14]. Accordingly, the amount of the diffusing nitrogen through the F1 sample was lower than that through the F2 sample. As a result, for the F1 nitrided samples, the formation of  $\text{Fe}_4\text{N}$  and  $\text{Fe}_{2-3}\text{N}$  phases seems to be attributed to the compound layer [14]. For the F2 samples, the  $\text{Fe}_4\text{N}$  phase belongs to both compound and diffusion layer due to the diffusion of nitrogen into the Fe(Si) phases and formation of the nitride phase according to the following reactions [16]:



The Si-N precipitates resulting from the disproportionation process of the  $\alpha$ -Fe(Si) phase were not detected. This is probably due either to their small size (the reaction thus occurring on a very fine scale) or to the fact that they could be amorphous, or both.

Treating at 440°C leads to the increase of the intensity of Fe(Si) phase in both annealed and nitrided F2 alloy as well as the iron nitrides in nitrided F2 alloy. The superlattice diffraction peaks of  $\text{Fe}_3\text{Si}$  were not in resolution range of the X-ray diffraction patterns.

The diffraction peak intensity of  $\text{Fe}_4\text{N}$  phase is higher for nitrided F2 alloy than F1 alloy. This could be

**Table 1.** Crystallization temperatures for F1 and F2 amorphous samples measured by DSC.

	Onset Temp. (°C)		Peak Temp. (°C)		Endset Temp. (°C)	
	First peak	Second peak	First peak	Second peak	First peak	Second peak
F2	426.03	557.07	435.79	563.51	451.36	566.96
F1 [13]	472.60	584.92	484.22	601.23	530.26	626.86

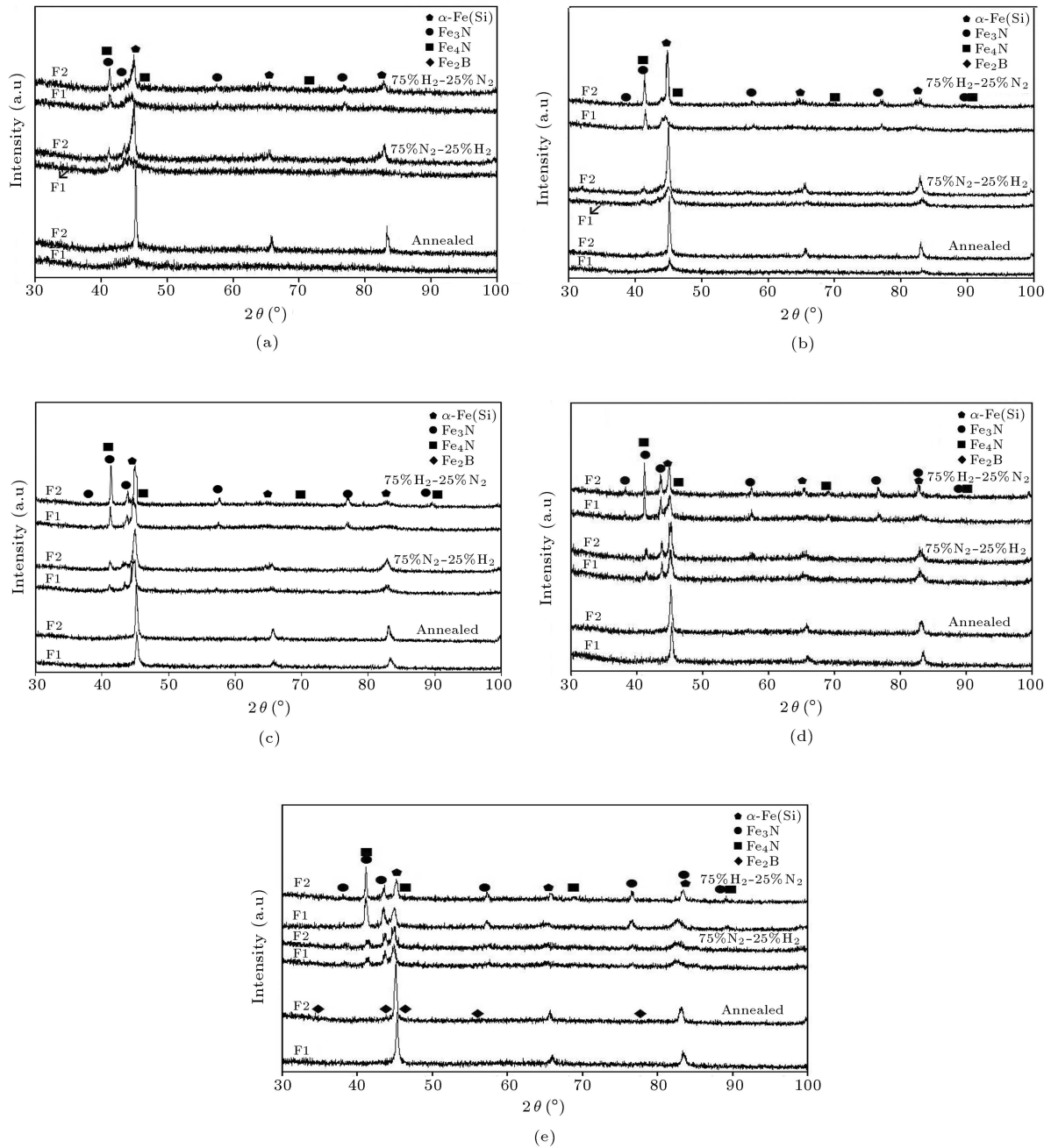


**Figure 3.** XRD patterns of the ASPN and annealed F1 and F2 ribbons at (a) 410°C, (b) 440°C, (c) 480°C, (d) 520°C and (e) 560°C for 3 h.

explained by the increasing content of such a phase due to the higher crystalline volume fraction, more nitrogen diffusion into the Fe(Si) phase and consequently, the formation of more Si-N and Fe<sub>4</sub>N nitrides for F2 alloy. In addition, in F1 alloy, higher amount of Nb content could be responsible for the slowing down of the nitrogen diffusion due to the formation of more nitrides such as Nb<sub>2</sub>N ( $\Delta H = -59.9$  Kcal/mol) and NbN ( $\Delta H = -56.2$  Kcal/mol) [16,17]. However, such nitrides have not been identified by the techniques used in this work. Annealing at higher temperatures not only leads

to grain growth of Fe(Si) phase, but also additional phases are formed from the amorphous matrix at 560°C for both alloys. This second stage of crystallization corresponds to the second peak in the DSC curve where boride phases are formed. These phases have higher intensity in F2 alloy compared to the F1 alloy, due to the lower second crystallization temperature for F2 alloy. The boride phases in nitrated F1 and F2 alloys disappeared which could be due to a nitrogenation reaction, in relation with the formation of Fe<sub>4</sub>N [14].

During the nitriding process, the active screen is

covered by a compound layer containing both  $\text{Fe}_4\text{N}$  and  $\text{Fe}_{2-3}\text{N}$  under normal nitriding conditions. Therefore, the sputtering target are more likely to be iron nitride ( $\text{Fe}_x\text{N}$  for  $x > 2$ ). These submicron nitride particles with a very high activity when passing through the plasma atmosphere, would physically and chemically adsorb the active nitrogen atoms, which are also in the plasma space. After the nitrogen rich particles deposited on the specimen surface, the physically adsorbed nitrogen atoms desorb because of the contact between the particles and the substrate surface and the high substrate temperature. The released nitrogen atoms will diffuse into the samples at the nitriding temperature. A part of the particles which adsorbed nitrogen atoms chemically combines to form nitrides such as  $\text{Fe}_{2-3}\text{N}$  and  $\text{Fe}_4\text{N}$  as a compound layer [13]. The SEM analysis confirmed the presence of the compound layer on the surface of the nitrided ribbon (Figure 4). As shown in Figure 3, the nitrided layer on the surface of the nitrided F1 and F2 ribbons in each temperature contains more  $\text{Fe}_4\text{N}$  than  $\text{Fe}_{2-3}\text{N}$  phase in 75%  $\text{H}_2$ -25%  $\text{N}_2$  gas mixture.

Using the Williamson-Hall procedure and eliminating the instrumental broadening of the diffraction lines, an average grain size of Fe(Si) phase for the F2 alloy was estimated. Figure 5 shows the average crystallites size as well as the crystalline fraction embedded in the amorphous matrix as functions of temperature. The higher value of the mean grain size for the F2 alloy, comparing to the F1 alloy [14] for the same nitriding and annealing conditions is induced by the lower Nb and Cu contents and crystallization temperature in F2 alloy. As could be seen, in both alloys, the mean grain

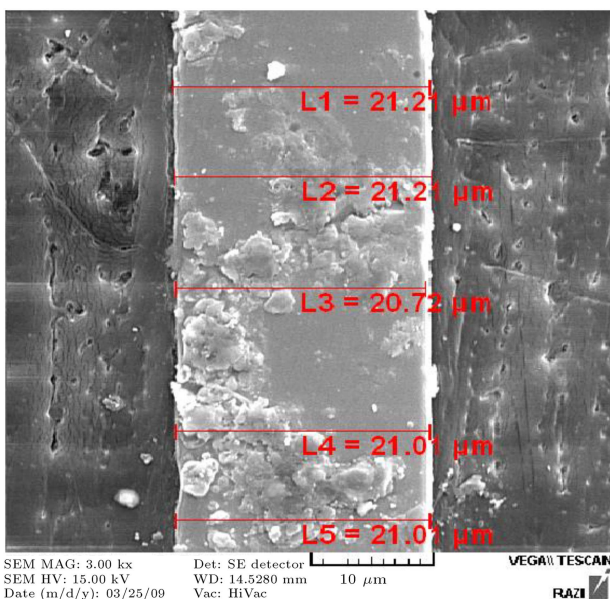


**Figure 4.** SEM images of the cross section of nitrided F2 ribbon at 410°C in 75%  $\text{H}_2$ -25%  $\text{N}_2$  gas mixture.

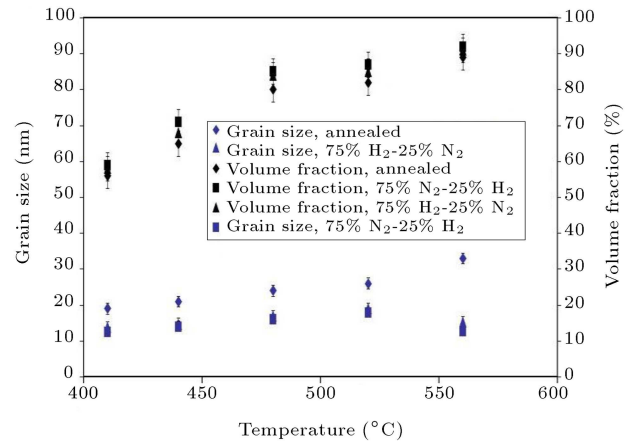


**Figure 5.** Average crystallites size of F2 alloy calculated from the X-ray diffraction patterns, and crystalline volume fraction of F2 alloy calculated from the areas of Bragg peaks using Rietveld refinement.

size of the Fe(Si) phase is smaller in nitrided samples compared to that of the annealed samples, which is the result of the introduction of nitrogen in the nitrided samples and the formation of Si-N precipitates. This suggests that ASPN treatment can give an improved nanocrystalline state in Finemet ribbons. Moreover, in 75%  $\text{N}_2$ -25%  $\text{H}_2$  gas mixture, the finer grain size obtained, which is due to the more nitrogen diffusion and Si-N precipitates. The crystalline volume fraction for the annealed and nitrided F2 alloy in each temperature is higher than that for the annealed and nitrided F1 alloy according to [14], which is due to the lower primary crystallization temperature for the F2 alloy. ASPN treatment results in an increase of volume fraction and as could be seen, the crystalline volume fraction for both nitrided samples in 75%  $\text{N}_2$ -25%  $\text{H}_2$  gas mixture is higher than that in 75%  $\text{H}_2$ -25%  $\text{N}_2$ . It has been found that nitrogenation affects the magnetostriction constant [18]. The value of  $\lambda_s$  is smaller for the nitrided samples than for the annealed samples. This is related to the higher crystalline volume fraction in the nitrided sample. The smaller grain size in the nitrided samples can also influence  $\lambda_s$  of the alloy [8].

Figure 6 shows that lattice parameter of the F2 alloy at its nanocrystalline state decreases with the increase of Si-content. Silicon which has small atomic radius, when dissolved in  $\alpha$ -Fe, reduces the lattice parameter value of pure  $\alpha$ -Fe phase [19]. Si content within Fe(Si) phase increases with the annealing temperature to 520°C and then decreases at 560°C (Figure 7). Annealing at 410°C results in the nanocrystallization of F2 alloy and Si solution in the Fe(Si) phase. But for F1 alloy, Fe(Si) nuclei are depleted from Si, whereas they could contain Cu atoms at this temperature [14,20]. Accordingly, the lattice parameter of Fe(Si) phase in annealed and nitrided F2 alloy is lower than that in annealed and nitrided

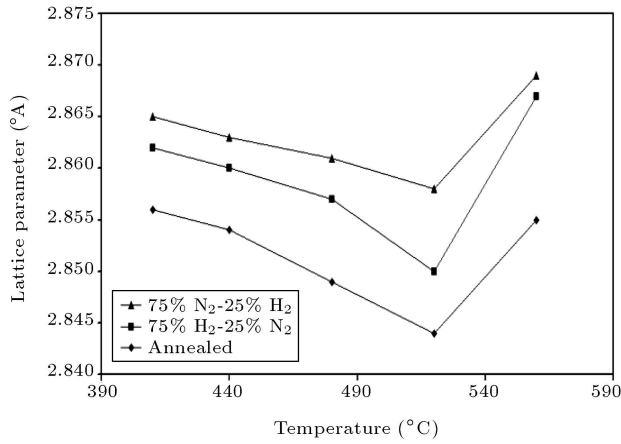


**Figure 6.** Variation of the lattice parameter Fe(Si) phase with the temperature for the nitrided and annealed F2 sample calculated from the XRD patterns. Estimated error is  $\pm 0.002 \text{ \AA}$ .

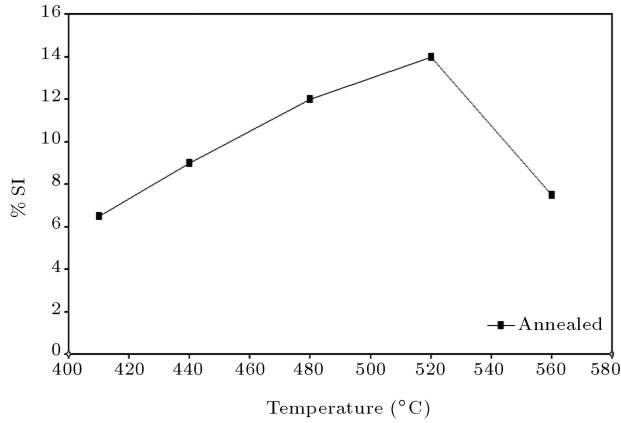


**Figure 7.** At %Si content in Fe(Si) for F2 alloy, estimated from the lattice parameters. Estimated error is  $\pm 1\%$ .

F1 alloy which was reported elsewhere [14]. But at 440°C and temperatures above, it exceeds in annealed and nitrided F2 alloy due to the lower Si content in the alloy and consequently in Fe(Si) phase. According to Figure 6, ASPN treatment causes an increase of the lattice parameter for a part of the Fe(Si) phase

where nitrogen has diffused. Moreover, the superior nitriding potential is demonstrated by the larger lattice parameter of that part of the Fe(Si) phase.

In the frame work of a simple geometrical model, the intergranular spacing was estimated (Table 2) using the average grain size and the amorphous volume fraction in the samples according to the following equation [8]:

$$\delta = P_{am}D/3. \quad (3)$$

The degree of dispersion of the nanograins inside the amorphous residual matrix is shown to be strongly dependent on the ribbons composition, mainly related to the Nb and Cu content [21]. For F2 alloy, the higher value of the intergranular spacing is a direct consequence of reduction of Nb and Cu contents which allow further growing of the nanograins formed during primary crystallization.

To know whether nitrided phases were coated on the surface and diffused into the ribbons, the concentration of alloying elements containing nitrogen were analyzed along the thickness direction using EDS (Table 3). As could be seen, EDS analysis shows the presence of Fe and N on the surface of the ribbons which is generally referred to the compound layer, but a low Si content on the surface could be detected except for 480°C and in 75% N<sub>2</sub>-25% H<sub>2</sub> gas mixture, indicating the discontinuous compound layer. EDS demonstrated the presence of Fe, Si and N in the diffusion zone. It is expected that the diffusion of nitrogen from the surface to the interior is observed depending on the temperature, time and the chemical composition of the base material [22]. The concentration of nitrogen in the compound layer is more than that of the diffusion zone. Comparing the nitrogen content of the surface and bulk of the nitrided F1 alloy with that of the nitrided F2 alloy, it could be seen that the nitrogen concentration on the surface of both ribbons with the same gas mixture are almost similar at 480°C and 560°C. But it is more for F2 alloy compared to F1 alloy in the bulk of the ribbons, since

**Table 2.** The intergranular distance for F1 and F2 alloys,  $\delta$  (nm)<sup>a</sup>.

Temperature (°C)	ASPN: 75% N <sub>2</sub> -25% H <sub>2</sub>		ASPN: 25% N <sub>2</sub> -75% H <sub>2</sub>		Annealed	
	F1	F2	F1	F2	F1	F2
410	0.90	1.71	0.97	1.93	1.00	2.79
440	0.85	1.35	1.05	1.58	1.24	2.45
480	0.63	0.80	0.74	0.91	1.21	1.60
520	0.6	0.64	0.76	0.78	1.17	1.56
560	0.27	0.34	0.33	0.46	0.88	1.21

a: Estimated error is  $\pm 0.05$  nm.

**Table 3.** EDS results for F1 and F2 nitrided ribbons<sup>a</sup>.

Surface								
ASPN	75% N <sub>2</sub> -25% H <sub>2</sub>				75% H <sub>2</sub> -25% N <sub>2</sub>			
Temperature (°C)	480		560		480		560	
Alloy	F1	F2	F1	F2	F1	F2	F1	F2
N (at %)	22.95	23.76	32.85	33.74	19.28	20.73	25.64	24.43
Fe (at %)	69.42	72.64	66.59	66.02	79.88	77.59	74.19	74.25
Si (at %)	7.63	3.6	0.56	0.24	0.84	1.68	0.33	1.32
Specific Distance from the Surface								
ASPN	75% N <sub>2</sub> -25% H <sub>2</sub>				75% H <sub>2</sub> -25% N <sub>2</sub>			
Temperature (°C)	480		560		480		560	
Alloy	F1	F2	F1	F2	F1	F2	F1	F2
N (at %)	15.29	19.64	18.99	24.18	11.35	17.25	15.53	18.53
Fe (at %)	75.04	76.24	77.34	73.55	83.44	79.88	77.44	78.08
Si (at %)	9.06	4.12	3.67	2.27	5.21	2.87	6.81	3.39
Center								
ASPN	75% N <sub>2</sub> -25% H <sub>2</sub>				75% H <sub>2</sub> -25% N <sub>2</sub>			
Temperature (°C)	480		560		480		560	
Alloy	F1	F2	F1	F2	F1	F2	F1	F2
N (at %)	3.86	5.51	5.69	5.8	1.97	3.10	5.32	5.39
Fe (at %)	85.81	88.13	85.59	88.08	89.06	89.77	86.53	88.47
Si (at %)	9.34	6.05	7.9	6.12	8.97	6.13	7.17	6.13

a: Estimated error is  $\pm 2\%$

F2 alloy contains higher crystalline volume fraction and lower amount of Nb content which could play a barrier role in diffusion of nitrogen because of the large atomic radius of niobium [8]. The second important result from Table 3 which deserves attention is that the nitrogen content on the surface of the ribbons for both alloys is higher in 75% N<sub>2</sub>-25% H<sub>2</sub> gas mixture than in 75% H<sub>2</sub>-25% N<sub>2</sub> in which it contains more

Fe<sub>2-3</sub>N phase than Fe<sub>4</sub>N according to the XRD results. Moreover, the nitrogen concentration in the bulk of both alloys increases with the increasing of the nitriding temperature and nitrogen content in the gas mixture.

Figure 8 shows AFM images of the surfaces of nitrided F1 and F2 alloys which according to the EDS results, corresponds to the iron nitrides. It is significant to note that the mean grain size of the iron nitrides on

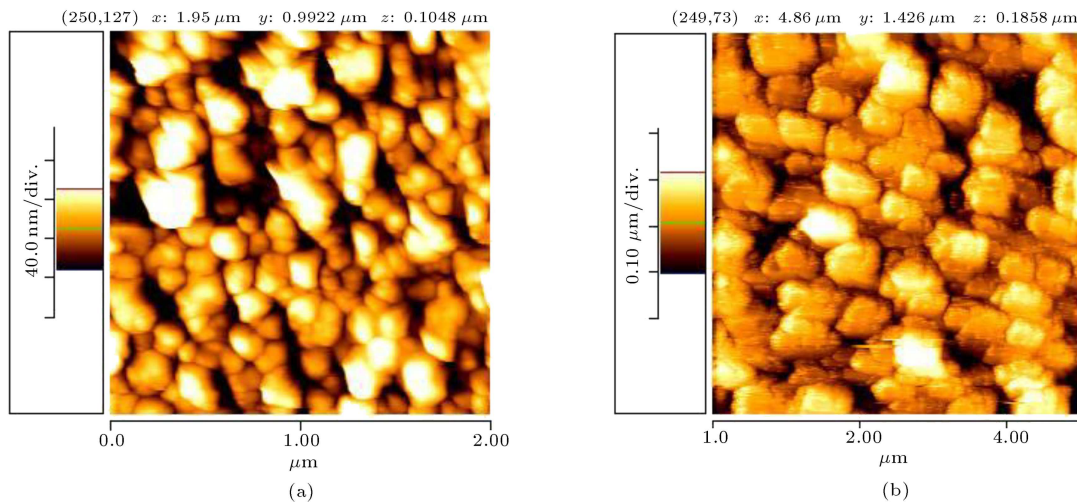


**Figure 8.** AFM surface images of the nitrided (a) F1 and (b) F2 ribbons in 75% N<sub>2</sub>-25% H<sub>2</sub> gas mixture at 520°C.

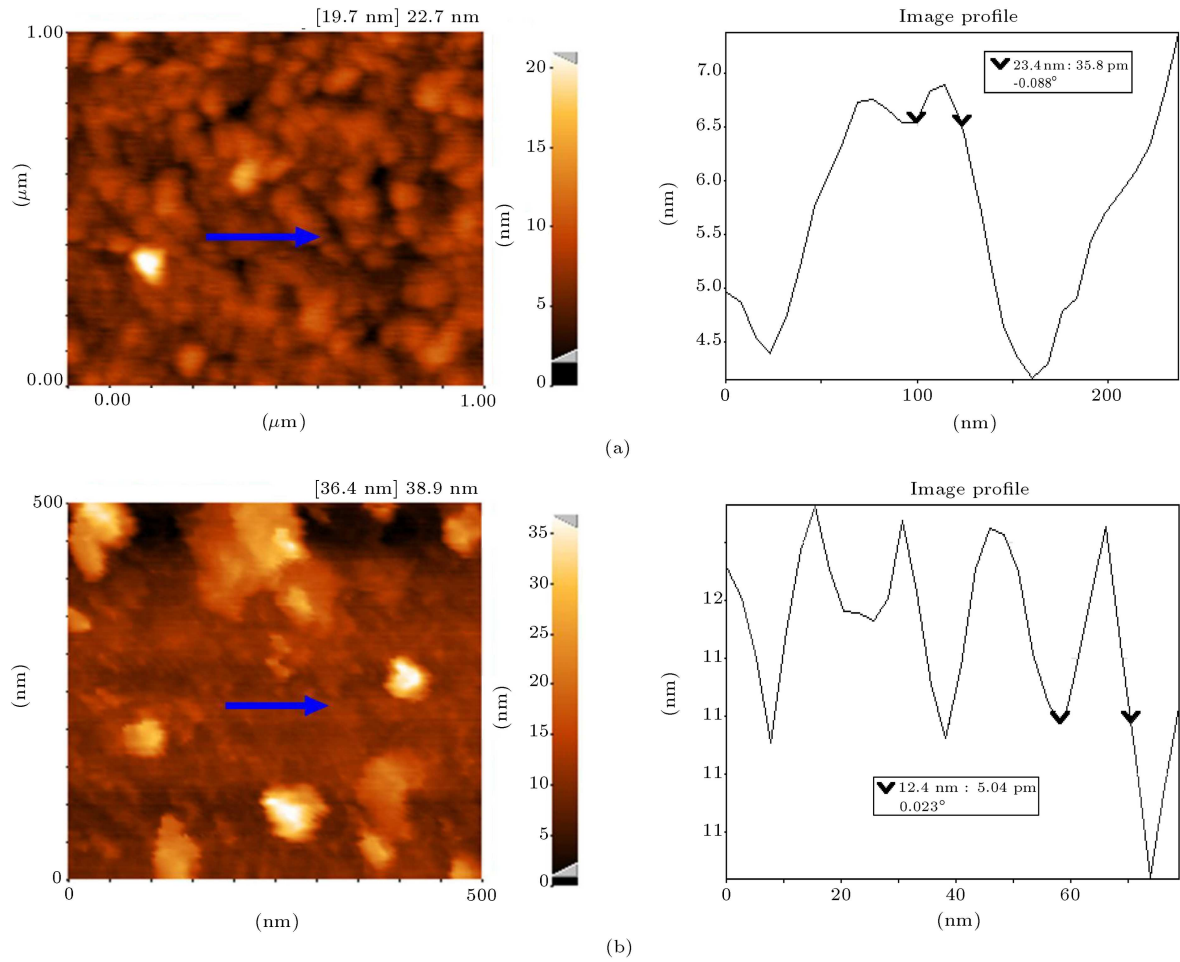


**Figure 9.** AFM images of the annealed (a) F2 and (b) F1 ribbons at 480°C.

the surface of the F1 alloy is smaller than that of the F2 alloy. It is probably due to the Si-N precipitates on the surface of the ribbons which act as nucleation centers. The more Si content in F1 alloy and, consequently, the more Si-N precipitates on the surface of the ribbons regarding the completion of nanocrystallization on the surface, lead to finer grain size of the iron nitrides. The images for annealed samples show that the crystallization at the surface level is fully completed (Figure 9); meanwhile in the XRD patterns there is no evidence of any reflection belonging to FeB phases which are the final products of the crystallization process. This fact confirms that the crystallization process is different in the surface of the samples than in the bulk. It is expected that crystallization process is quicker at the surface [23]. The mean grain size of these nanograins and nitrides estimated from AFM images are compared with the corresponding one obtained by XRD patterns, achieving a good agreement between the two techniques in both cases.

Figure 10 shows the electrical resistivity of the annealed and nitrided F2 alloy. For comparison of both alloys, it can be noted that the grain size of Fe(Si) phase

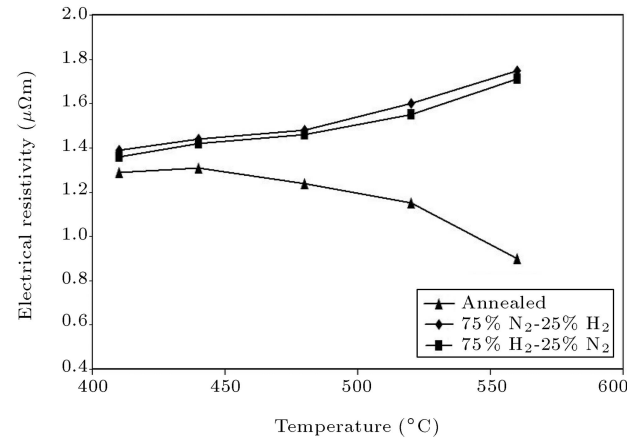


**Figure 10.** Temperature dependence of the electrical resistivity for F2 alloy.

and the Si content within Fe(Si) play a vital role in the resistivity at nanostate where nanoparticles of Fe(Si) are dispersed in amorphous matrix [19]. Accordingly, the decrease of electrical resistivity for the annealed and nitrided F2 alloy compared to the F1 alloy [14] at temperatures above 410°C is due to the larger grain size

and lower Si content in Fe(Si) phase of this alloy. At 410°C, resistivity is lower for the annealed and nitrided F1 alloy [14], although particle size of the nanophase is smaller than that for the annealed and nitrided F2 alloy. It is due to the lower Si content in Fe(Si) nuclei for both annealed and nitrided F1 alloy and the absence of the nitrided phases in the diffusion layer of nitrided F1 alloy. After formation of nanocrystalline phase, resistivity is found to be increased. It is generally accounted that in nanocrystalline alloys, the rise in resistivity after nanocrystallization is due to the grain boundary scattering by the crystallization and nanoparticles [19]. The formation of boride phases such as Fe<sub>2</sub>B and full nanocrystallization in the annealed F2 alloy are responsible for the decrease in resistivity. Also for both nitrided ribbons, the electrical resistivity is higher than that for the annealed samples due to the formation of iron nitrides and nitrided phases such as Si-N precipitates, Nb<sub>2</sub>N and NbN which have high electrical resistivity. In contrast to the annealed samples, electrical resistivity increases at higher temperatures in the nitrided samples.

Figure 11 shows the plot of hardness versus temperature from the bulk of the F2 ribbon. The increase in hardness for F2 alloy compared to the F1 alloy at 410°C is mainly due to the nanocrystallization process and presence of Fe(Si) phase with nanometric grains. As annealing temperature increases to 520°C, hardness values increase for both alloys. But the larger grain size of Fe(Si) phase and higher crystalline volume fraction in F2 alloy result in a higher hardness value than F1 alloy [14]. At 560°C, more decrease of the hardness value could be seen for F2 alloy due to the lower second crystallization temperature and consequently, more grain growth. In ASPN treatment, nitrogen is mainly incorporated into the existing iron lattice as interstitial atoms or as finely dispersed alloy nitride precipitates. It is possible to say that hardening

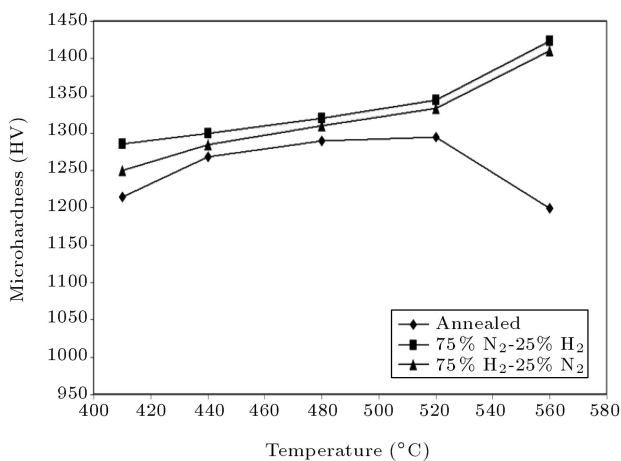


**Figure 11.** Bulk micro-hardness versus temperature for F2 alloy.

in the diffusion layer is caused by the microstrain in the matrix induced by the formation of coherent precipitated phase [15]. Moreover, nitrogen atoms located in interstitial positions cause solid solution hardening, thus increase the hardness of the samples. The higher amount of hardness value for nitrided F2 alloy, compared to the F1 alloy, is due to the same reasons mentioned for the annealed samples and also the more nitrogen diffusion into the F2 ribbons as well as the formation of more Fe<sub>4</sub>N phase.

The magnetic properties in the nanocrystalline FeSiNbBCu alloys are dominated by the structure which depends on compositions and annealing conditions. It is significant for application to improve the soft magnetic properties in the nanostructured FeSiNbBCu alloys with high saturation magnetization ( $M_s$ ) [23]. The room temperature hysteresis loops of F2 alloy were measured (Figure 12). As shown, both the coercivity ( $H_c$ ) and  $M_s$  increase after the nitrification process. The  $M_s$  of the heat treated F2 sample was, however, higher than that of the F1 sample which has been previously reported [14]. This is related to the higher Fe content in F2 alloy. The formation of more Fe<sub>4</sub>N nitrides also leads to the increase of  $M_s$  for the nitrided F2 alloy, compared to the nitrided F1 alloy. As could be seen, for nitrided F2 alloy, by using 75% H<sub>2</sub>-25% N<sub>2</sub> gas mixture,  $M_s$  is higher with respect to 75% N<sub>2</sub>-25% H<sub>2</sub> gas mixture. It is interesting to note that the  $H_c$  of the samples containing Fe<sub>3</sub>Si phase is lower by an order of magnitude, as compared to the samples containing  $\alpha$ -Fe(Si) phase [5]. Accordingly, the  $H_c$  decreases with increasing Si content in amorphous and partially crystallized phases. Due to this fact, it increases from F1 to F2 alloy in both annealed and nitrided samples. At 440°C, despite the nitrided F1 sample, the  $H_c$  is higher in nitrided F2 sample with higher amount of nitrogen content in the nitriding gas mixture. At this temperature, the nanocrystallization

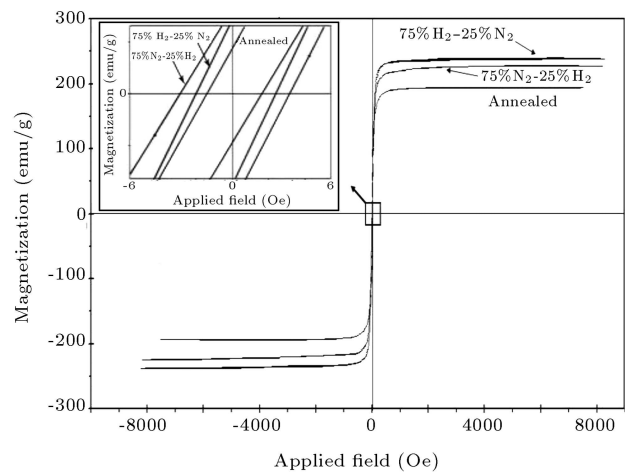


**Figure 12.** Magnetization curve for nitrided and annealed F2 at 440°C.

**Table 4.** The values of  $M_s$  and  $H_c$  for different samples at 440°C.

Coercivity (Oe)	ASPN: 75% N <sub>2</sub> -25% H <sub>2</sub>		ASPN: 75% H <sub>2</sub> -25% N <sub>2</sub>		Annealed	
	F1 [13]	F2	F1 [13]	F2	F1 [13]	F2
	1.5	5	3.4	4	1.2	2
Saturation Magnetization (emu/g)	110	225	119	239	105	195

of Fe(Si) phase, diffusion of nitrogen into the Fe(Si) grains and, therefore, the formation of Fe<sub>4</sub>N nitrides take place. These could be resulted in the higher amount of  $H_c$  for F2 nitrided in 75% N<sub>2</sub>-25% H<sub>2</sub> gas mixture than that in 75% H<sub>2</sub>-25% N<sub>2</sub>. But for F1 nitrided in 75% H<sub>2</sub>-25% N<sub>2</sub> gas mixture,  $H_c$  is more than that in 75% N<sub>2</sub>-25% H<sub>2</sub> gas mixture. The values of  $M_s$  and  $H_c$  for F1 and F2 alloys are presented in Table 4.

## CONCLUSIONS

1. A comparative study of nanocrystallization of two series of Finemet alloys with different compositions after active screen plasma nitriding and annealing at different temperatures was made. Nitriding of Fe<sub>77.5</sub>Si<sub>13.5</sub>B<sub>9</sub>Nb<sub>3</sub>Cu<sub>1</sub> and Fe<sub>77</sub>Si<sub>11</sub>B<sub>9</sub>Nb<sub>2.4</sub>Cu<sub>0.6</sub> alloys led to the decrease of Fe(Si) grain size and increase of the crystalline volume fraction.
2. The smaller amount of Nb shifted the onset crystallization temperatures towards lower temperatures, leading to the larger grain size of Fe(Si) phase and higher crystalline volume fraction in each temperature for both nitrided and annealed Fe<sub>77</sub>Si<sub>11</sub>B<sub>9</sub>Nb<sub>2.4</sub>Cu<sub>0.6</sub> samples compared to Fe<sub>73.5</sub>Si<sub>13.5</sub>B<sub>9</sub>Nb<sub>3</sub>Cu<sub>1</sub> alloy.
3. ASPN treatment caused an increase of the lattice parameter for a part of the Fe(Si) phase where nitrogen has diffused. The superior nitriding potential is demonstrated by the larger lattice parameter of that part of the Fe(Si) phase. At temperatures which the nanocrystallization of both alloys takes place, the lattice parameter of Fe(Si) phase for Fe<sub>77</sub>Si<sub>11</sub>B<sub>9</sub>Nb<sub>2.4</sub>Cu<sub>0.6</sub> alloy was larger than that for Fe<sub>73.5</sub>Si<sub>13.5</sub>B<sub>9</sub>Nb<sub>3</sub>Cu<sub>1</sub> alloy due to the lower Si content in Fe<sub>77</sub>Si<sub>11</sub>B<sub>9</sub>Nb<sub>2.4</sub>Cu<sub>0.6</sub> alloy and consequently, in Fe(Si) phase.
4. The mean grain size of the iron nitrides on the surface of the Fe<sub>73.5</sub>Si<sub>13.5</sub>B<sub>9</sub>Nb<sub>3</sub>Cu<sub>1</sub> alloy was smaller than that of the Fe<sub>77</sub>Si<sub>11</sub>B<sub>9</sub>Nb<sub>2.4</sub>Cu<sub>0.6</sub> alloy. It is believed that this is related to the higher amount of Si-N precipitates as a nucleation centers on the surface of the Fe<sub>73.5</sub>Si<sub>13.5</sub>B<sub>9</sub>Nb<sub>3</sub>Cu<sub>1</sub> ribbons.
5. ASPN treatment increased the electrical resistivity of alloys. The larger grain size and lower Si content

in Fe(Si) phase for Fe<sub>77</sub>Si<sub>11</sub>B<sub>9</sub>Nb<sub>2.4</sub>Cu<sub>0.6</sub> alloy gave rise to a decrease of electrical resistivity compared to Fe<sub>73.5</sub>Si<sub>13.5</sub>B<sub>9</sub>Nb<sub>3</sub>Cu<sub>1</sub> alloy.

6. It was concluded that nitriding increased the hardness of alloys. The highest hardness was achieved for nitrided Fe<sub>77</sub>Si<sub>11</sub>B<sub>9</sub>Nb<sub>2.4</sub>Cu<sub>0.6</sub> alloy at 560°C in 75% N<sub>2</sub>-25% H<sub>2</sub> gas mixture.
7. Comparison of magnetic results for both alloys showed that the maximum saturation magnetization and coercivity were obtained for Fe<sub>77</sub>Si<sub>11</sub>B<sub>9</sub>Nb<sub>2.4</sub>Cu<sub>0.6</sub> alloy after nitriding under 75% H<sub>2</sub>-25% N<sub>2</sub> and 75% N<sub>2</sub>-25% H<sub>2</sub> gas mixture at 440°C, respectively.

## REFERENCES

1. Ferna'ndez, L. et al. "Magnetic behavior and microstructure of Finemet-type ribbons in both, surface and bulk", *Journal of Non-Crystalline Solids*, **353**, pp. 777-781 (2007).
2. Manivel Raja, M. et al. "Structure and soft magnetic properties of Finemet alloys", *Journal of Alloys and Compounds*, **297**, pp. 199-205 (2000).
3. Herzer, G., *Handbook of Magnetic Materials*, K.H.J. Buschow, Eds., **10**, pp. 415-462, Elsevier, Amsterdam (1997).
4. Raszka, T. and Przybyl, A. "Optimisation of soft magnetic properties in Fe<sub>83-x</sub>Co<sub>x</sub>Nb<sub>3</sub>B<sub>13</sub>Cu<sub>1</sub> (x=10, 30, 40) amorphous alloys", *13th International Scientific Conference on Achievements in Mechanical and Materials Engineering*, Gliwice, Poland, 16th-18th May (2005).
5. Majumdar, B. and Akhtar, D. "Structure and coercivity of nanocrystalline Fe-Si-B-Nb-Cu alloys", *Journal of Bull. Mater. Sci.*, **28**(5), pp. 395-399 (2005).
6. Li, C. et al. "Crystallization behavior of co-containing FINEMET amorphous alloy melt-spun ribbon", *Journal of Materials Letters*, **60**, pp. 309-312 (2006).
7. Iturriza, N. et al. "Nanostructure and magnetic properties of Ni-substituted Finemet ribbons", *Journal of Magnetism and Magnetic Materials*, **316**(2), pp. 74-77 (2007).
8. Atmani, H. et al. "Crystallization-nitriding process of FeSiB and FeSiBCuNb ribbons: Influence of additive (Cu, Nb) pair and nitrogen on structure magnetic

- and magnetostrictive parameters”, *Journal of Non-Crystalline Solids*, **290**, pp. 194-207 (2001).
9. Atmani, H. and Thoumire, O. “Microstructure characterization of fluidized bed nitride Fe-Si and Fe-Si-Al foils”, *Bull. Mater. Sci.*, **25**, pp. 219-225 (2002).
  10. Alves, C. Jr. et al. “Use of cathodic cage in plasma nitriding”, *Journal of Surface Coating & Technology*, **201**, pp. 2450-2454 (2006).
  11. Wang, L. et al. “Plasma nitriding of low alloy steels at floating and cathodic potentials”, *Journal of Applied Surface Science*, **254**, pp. 6595-6600 (2008).
  12. de Sousa, R.R.M. et al. “Cathodic cage nitriding of samples with different dimensions”, *Journal of Material Science and Engineering A*, **465**, pp. 223-227 (2007).
  13. Zhao, C. et al. “Study on the activate plasma nitriding and its nitriding mechanism”, *Journal of Surface & Coatings Technology*, **201**, pp. 2320-2325 (2006).
  14. Shivaee, H.A. et al. “Study of nanocrystallization in FINEMET alloy by active screen plasma nitriding”, *Journal of Alloys and Compound*, **491**(1-2), pp. 487-494 (2009).
  15. Turk, A. et al. “Structural characterization of fluidized bed nitrided steels”, *Journal of Vacuum*, **80**, pp. 332-342 (2005).
  16. Grognet, S. et al. “Microstructural study of nanocrystalline Fe-(Cu-Nb)-Si-B ribbons obtained by a nitriding thermochemical treatment”, *Journal of Magnetism and Magnetic Materials*, **210**, pp. 167-180 (2000).
  17. Atmani, H. et al. “Nitriding thermochemical treatment and Niobium dual effect on nanocrystallization FeSi-BCu ribbons”, *Journal of Scripta Mater.*, **42**, pp. 117-122 (2000).
  18. Grognet, S. et al. “The influence of nitrogen on the structural and magnetic properties of nanocrystallized Finemet-type ribbons”, *Journal of Magnetism and Magnetic Materials*, **203**, pp. 172-174 (1999).
  19. Panda, A.K. et al. “Crystallization and soft magnetic properties of rapidly solidified  $Fe_{73.5}Nb_3Cu_1Si_{22.5-X}B_X$  ( $X=5,9,10,11,19$ ) alloys”, *Journal of Magnetism and Magnetic Materials*, **260**, pp. 70-77 (2003).
  20. Cziráki, Á. et al. “Some structural aspects of magnetic property evolution in Finemet-type sensor material during amorphous-nanocrystalline transformations”, *Journal of Periodica Polytechnica Ser. Transp. Eng.*, **47**, pp. 167-176 (2004).
  21. Crisan, O. et al. “Nanocrystallization of soft magnetic Finemet-type amorphous ribbons”, *Journal of Sensors and Actuators A*, **106**, pp. 246-250 (2003).
  22. Usta, M. et al. “Nitriding of AISI 316L surgical stainless steel in fluidized bed reactor”, *Journal of Vacuum*, **73**, pp. 505-510 (2004).
  23. Yoshizawa, Y. “Magnetic properties and applications of nanostructured soft magnetic materials”, *Journal of Scripta Mater.*, **44**, pp. 1321-1325 (2001).

## BIOGRAPHIES

**Elmira Memarzadeh Lotfabad** completed his B.S. and M.S. studies in the Materials Science and Engineering at Tehran University and Sharif University of Technology, respectively, in 2009. She is currently working on research papers in the field of Nanostructures. She has ranked 1th among all M.S. Materials Selection and Processing students based on overall GPA at Sharif University of Technology.

**Hamid Reza Madaah Hosseini** is a professor of Materials Science and Engineering at Sharif University of Technology. He received his Ph.D. in Advanced Materials from Sharif University of Technology in 2000 and was appointed as a member of Scientific Committee in the Department. He is currently working as a member in Institute for Nanoscience and Nanotechnology at Sharif University of Technology. His field of research is Magnetic Materials and Nanostructures and has published a lot of papers in this field.

**Hossein Asghari Shivaee** received his B.S. in the Mining and Metallurgical Engineering from Amir Kabir University of Technology in 2002 and M.S. and Ph.D. in Nanoscience and Technology-Nanomaterials from Sharif University of Technology in 2010. He is currently working in Institute for Nanoscience and Nanotechnology and doing some research work in the field of Nanotechnology.

**Saied Roostaie** received his B.S. in the Mining and Metallurgical Engineering in 2002 from Amir Kabir University of Technology. He is currently working in Research Centers related to Metallurgical Engineering in Tehran.